Above-surface neutralization of slow highly charged ions in front of ionic crystals

Lotten Hägg,[1,2] Carlos O. Reinhold,[2,3] and Joachim Burgdörfer[2,3]
[1]*Atomic Physics, Stockholm University, Frescativ. 24, S-104 05 Stockholm, Sweden*
[2]*University of Tennessee, Department of Physics and Astronomy, Knoxville, Tennessee 37996-1200*
[3]*Oak Ridge National Laboratory, Oak Ridge, Tennessee 37831-6373*
(Received 11 October 1996)

We present a theoretical analysis of the above-surface neutralization of highly charged ions in front of LiF. The study is based on the assumption that the dominant electron transfer occurs in the classically allowed region. Estimates of critical distances and corresponding quantum numbers for capture from an ionic crystal within the classical-overbarrier (COB) model are presented, which differ considerably from corresponding results for metals. The role of the dielectric response of LiF is investigated. In addition, classical-trajectory simulations are performed for a slow highly charged ion approaching an insulator. It is shown that capture effectively begins $\sim$ 3 a.u. closer to the surface than estimated from the COB model. This correction can be incorporated into a modified COB model. The energy gain for grazing incidence ions is obtained using a staircase model which includes the deceleration due to charge-up of the surface. [S1050-2947(97)08503-X]

PACS number(s): 34.50.Dy, 34.70.+e, 79.20.Rf

I. INTRODUCTION

The interaction of slow highly charged ions (HCIs) with metal surfaces has been extensively studied, experimentally as well as theoretically, over the past few years [1–4], stimulated by the development of modern high current ion sources. More recently, there has been an increased interest in HCIs impinging on insulator surfaces [5–11], in particular, LiF. Possible technological applications include etching of surfaces of insulators and semiconductors with slow HCIs, which could be useful in the fabrication of microelectronic devices and nanostructures.

The microscopic processes involved during the interaction of HCIs with surfaces are of many-body nature and include multielectron transitions. From numerous studies of electron yields, soft x-ray emission, and scattered ions, the following scenario for the neutralization of HCIs near metals has emerged: As the HCI approaches the surface, it induces a rearrangement of the electron density in the solid (i.e., an ''image'') which, in turn, accelerates the ion towards the surface. This is known as image acceleration and the resulting energy change as image energy gain. As soon as the potential barrier separating the electronic motion in the surface and in the ion becomes lower than the Fermi edge, electrons are transferred in classical-overbarrier (COB) transitions between the metal and the ion. Under barrier transitions (tunneling) have been found to be negligible [2,4] for slow HCIs, with typical interaction times around $\sim 10^{-14}$ s. The interaction time is determined by the inverse perpendicular velocity of the HCI, which has a lower bound given by the image energy gain. The neutralization occurs by electron transfer into highly excited levels of the ion, leading to the formation of so-called ''hollow atoms.'' A COB model, which was originally developed for ion-atom collisions [12–14], was extended and used for HCI-metal surface interactions [2–4]. In spite of its inherent simplifications the COB model could explain the transient above-surface neutralization of an HCI near a metal, in particular the above-surface component of the K Auger emission [15] and the image energy gain. It also indicated that the atom remains hollow above the surface, i.e., the relaxation to the neutral ground state takes place only in close collisions with surface and below-surface layers of the solid.

Current experimental studies of HCIs impinging on insulator surfaces [5–11] seek to understand differences and similarities with the neutralization of HCIs near metals. Insulators have a narrow valence band, a large work function W, and a wide band gap Δ. In the case of LiF, which we focus on in the following, Δ even exceeds the work function ($\Delta > W$) extending into the positive-energy continuum. Furthermore, the dielectric response of a LiF surface strongly differs from that of a metal. First experimental results for HCIs incident on LiF have shown both similarities and differences to metals which are not yet well understood: the image energy gain in grazing incidence scattering was found to be similar to that of metals [5,6]. However, the KLL Auger peak with the minimal L population, signifying the hollow atom formation by above-surface neutralization for metals, was found to be missing [7], suggesting that hollow-atom formation is suppressed. Recent experiments on a different type of insulator, SiO_2, suggest, on the other hand, hollow-ion formation [11].

The present work attempts a theoretical description of the interaction between HCIs and insulator surfaces, more specifically, ionic crystals with applications to LiF. Our analysis makes use of realistic electronic potentials near an insulator whose response is treated using the experimental frequency-dependent dielectric function. Results for the first capture of an electron from the surface into an HCI are presented. We describe the charge transfer in terms of the classical-overbarrier (COB) model modified for insulator surfaces and give critical distances R_c for the onset of electron capture and critical n quantum numbers, n_c, for the projectile state the first electron is captured into. In addition, we have developed a classical-trajectory Monte Carlo (CTMC) approach [16,17] for this problem. In our classical-trajectory simulation the evolution of an electron, originating in a localized state in F^-, is followed during its removal from the LiF

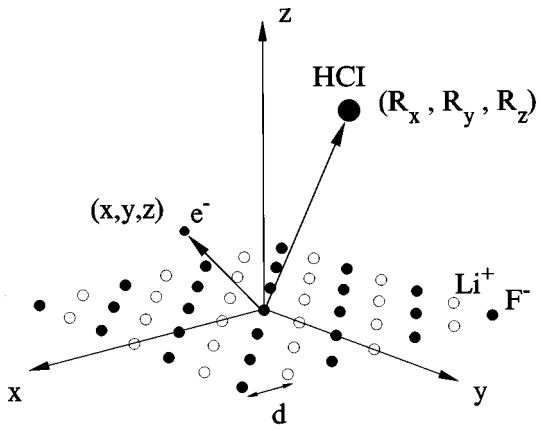

FIG. 1. Sketch of the coordinate system with the origin at an F^- ion in the LiF surface. The filled circles in the surface are F^- ions and the open circles Li^+ ions. The projectile is positioned at (R_x,R_y,R_z) outside the ionic crystal while the active electron has coordinates (x,y,z). The nearest-neighbor distance [for LiF(100) the distance between Li and F] in the crystal is denoted with d.

crystal due to the presence of the HCI. From the CTMC simulation we obtain estimates of capture and loss between the HCI and LiF. While this simulation is carried out only for the first electron transfer of the neutralization sequence, the present results are used to extrapolate to the complete neutralization sequence for grazing incidence. This permits an estimate of the image energy gain for HCIs approaching a LiF surface at grazing incidence. In the calculation of the total energy change of the HCI we also account for the deceleration caused by the charge-up of the surface from sequential removal of electrons. Differences to metallic targets in terms of velocity and charge dependencies are analyzed. In the following, atomic units are utilized unless otherwise stated.

II. THE ELECTRONIC SURFACE POTENTIAL

A realistic surface potential for an electron crossing the barrier between an ion and an ionic crystal can be written as

$$V(\vec{r},\vec{R})=V_e(\vec{r})+V_{pe}^I(\vec{r},\vec{R})+V_{pe}(\vec{r},\vec{R}), \tag{1}$$

where $\vec{r}=(x,y,z)$ is the position of the electron, with x and y parallel to the surface and z perpendicular to the surface, and $\vec{R}=(R_x,R_y,R_z)$ is the position of the projectile (an HCI). The origin of the coordinate system is chosen at a halide ion in the surface (F^- in LiF). A sketch of the geometry is given in Fig. 1. Although the following is valid for any ionic crystal, the discussion will focus on LiF.

In Eq. (1) the interaction between the electron and the image of the projectile is given by $V_{pe}^I(\vec{r},\vec{R})$, while $V_{pe}(\vec{r},\vec{R})$ is the Coulomb interaction between the electron and the projectile itself, and $V_e(\vec{r})$ is the electronic surface potential in absence of the perturbation by the HCI. The latter contains four terms,

$$V_e(\vec{r})=V_{pol}(\vec{r})+V_M(\vec{r})+V_{sc}(\vec{r})+V_e^{SI}(z), \tag{2}$$

representing the polarization potential $V_{pol}(\vec{r})$, which describes the interaction between the electron and the halide atom; the Madelung potential $V_M(\vec{r})$, which is the interaction between the electron and the ionic lattice of the crystal; $V_{sc}(\vec{r})$, which accounts for the screening of the localized positive charge left in the surface; and $V_e^{SI}(z)$, the interaction between the electron and its own image.

The attractive potential determining the affinity of F^- can be described by the induced polarization potential,

$$V_{pol}(\vec{r})=\frac{-\alpha_{pol}}{2(|\vec{r}|^2+c^2)^2}, \tag{3}$$

where $\alpha_{pol}=5.1$ a.u. is the dipole polarizability of the F atom [18] and c serves as a ''cutoff'' for small $|\vec{r}|$. Equation (3) leads to the correct asymptotic behavior

$$\lim_{|\vec{r}|\to\infty} V_{pol}(\vec{r})=\frac{-\alpha_{pol}}{2|\vec{r}|^4} \tag{4}$$

at large distances. The value $c=0.5664$ a.u. is obtained by solving the one-electron Schrödinger equation with V_{pol} such that the eigenenergy of an electron with angular momentum $l=1$ (the outermost electron in F^- is in a $2p$ orbital) is equal to the electron affinity of the F^- ion in vacuum, $E=-0.125$ a.u. [18].

The electrostatic interaction in an ionic crystal is a sum of Coulomb potentials between negatively charged and positively charged ions. This so-called Madelung potential, at an ionic site in the crystal, can be written as $-Mq_0^2/d$, where $\pm q_0$ is the charge of the ions, d is the nearest-neighbor spacing in the crystal, and M is called a Madelung constant [19–21]. While d is specific for each crystal ($d=3.8$ a.u. for LiF), M is specific for each crystal *structure*. For crystals with NaCl structure (such as LiF) $M=1.75$ in the bulk and 1.68 at the surface [for a (100) surface] [20]. In calculations of equilibrium properties for alkali halides Wang *et al.* [22] accounted for effects of fractional ionicity (i.e., $q_0\leqslant 1$). By comparing the theoretical results with experimental values, they concluded that for LiF $q_0\simeq\pm 0.86$.

Here, the Madelung sum is the sum of the Coulomb interactions between an electron with an effective charge $q(z)$ at a position $\vec{r}$ (which lies, in general, outside the crystal) and the ions in the crystal at positions $\vec{\mathcal{R}}_k$ and with charges $Z_k=\pm q(z)$. The origin of the electron is assumed to be at an F^- ion in the surface ($\mathcal{R}_k=0$) and the Madelung potential is

$$V_M(\vec{r})=\sum_{\mathcal{R}_k\neq 0}\frac{q(z)Z_k}{|\vec{r}-\vec{\mathcal{R}}_k|}. \tag{5}$$

The varying charge $q(z)$ accounts for the fractional ionicity in the surface ($z=0$) as discussed by Wang *et al.* [22]. We choose

$$q(z)=q_0+(q_\infty-q_0)f(z) \tag{6}$$

with the limits

$$\lim_{z\to 0}[q(z)]=q_0=0.86, \quad \lim_{z\to\infty}[q(z)]=q_\infty=1 \tag{7}$$

using

$$f(z)=\{1-\exp(-2z/3)\}^3 \quad (z\geqslant 0), \quad f(z)=0 \quad (z<0). \tag{8}$$

It is important that the inclusion of a z-dependent charge $q(z)$ does not introduce any force at the surface (i.e., $\partial q/\partial z=0$ at $z=0$), and our choice of $f(z)$ is consistent with this criterion. The explicit form of the switching function $f(z)$ is not crucial for the conclusions about first capture to be drawn later in this work.

The exact value of the Madelung sum $V_M(\vec{r})$ should be calculated for an infinite crystal [19–21]. However, if sufficient care is taken to ensure convergence, a finite number of rows and layers can for our purposes be used without significant loss of accuracy. As few as about 20 rows (x and y direction in the surface plane) and around 10 layers ($-z$ direction opposite to surface normal) are found to be sufficient. It is worth noting that if, for LiF, the electron affinity ($\sim$ 3.4 eV) is added to the Madelung potential ($\sim$8.9 eV), one obtains a total removal energy of an electron from LiF of 12.3 eV which is very close to the experimental work function which is about 12 eV [23,24].

In an analysis of first capture the long-range behavior of the potentials is of particular interest. For this purpose we define a function

$$a_M(z)\equiv -z, \quad V_M(x=0,y=0,z)/q^2(z) \tag{9}$$

for $z\geqslant 0$. The asymptotic limit ($z\gg 1$) is $a_M(z)\simeq 1$, implying that the long-range behavior of the Madelung potential is Coulombic, and we also note that by definition $a_M(0)=0$.

In order to calculate the potentials $V_{sc}(\vec{r})$, $V_e^{SI}(z)$, and $V_{pe}^I(\vec{r},\vec{R})$, it is necessary to treat the dynamic response of the crystal through the inclusion of a frequency-dependent dielectric function. The standard expression [4,25], derived within linear response and the specular reflection model, for the image potential induced by the ion with charge Q and experienced by an electron with charge $q(z)$ above the surface ($z>0$) is

$$V_{pe}^I(\vec{r},\vec{R}) = \frac{Qq(z)}{2\pi^2|v_z|}\int d\vec{K}\int d\omega\,\frac{v_z^2 e^{i(\vec{K}\cdot\vec{\rho}-\omega t)}}{v_z^2K^2+\overline{\omega^2}}\left[\frac{\epsilon(\omega)-1}{\epsilon(\omega)+1}\right]e^{-K|z|}, \tag{10}$$

with $\vec{r}=(\vec{\rho},z)$, $\vec{k}=(\vec{K},k_z)$, and $\vec{v}=(\vec{v}_{||},-v_z)$, where $\vec{k}$ is the wave vector and $\vec{v}$ is the velocity of the projectile (which follows a trajectory $\vec{R}(t)=\vec{v}t$). Furthermore, $\overline{\omega}=\omega-\vec{K}\cdot\vec{v}_{||}$, where ω is the frequency entering the dispersion independent dielectric function $\epsilon(\omega)$. The usage of a dielectric function without dispersion $\epsilon(\omega)=\epsilon(k=0,\omega)$ results in the image plane coinciding with the topmost layer of the crystal. The latter approximation could be eliminated if data on the dispersion were available. We note that the exact position of the image plane is not crucial for the determination of critical distances for capture, because of the dominance of the Madelung potential over the image contributions.

Equation (10) can be solved exactly for constant $\epsilon(\omega)=\epsilon$, which gives

$$V_{pe}^I(\vec{r},\vec{R})=\frac{(\epsilon-1)}{(\epsilon+1)}\frac{Qq(z)}{|\vec{r}-\vec{R}_I|}, \tag{11}$$

where $\vec{R}_I=(R_x,R_y,-R_z)$ is the position of the image of the ion. For a frequency-dependent dielectric function such a functional form is only obtained at very large distances and is known as the ''static'' or zero-frequency limit

$$V_{pe}^I(\vec{r},\vec{R})\xrightarrow[z,R_z\to+\infty]{}\frac{(\epsilon(0)-1)}{(\epsilon(0)+1)}\frac{Q}{|\vec{r}-\vec{R}_I|}. \tag{12}$$

A major difference between a metal and an insulator is the behavior of the dielectric function $\epsilon(\omega)$ in the limit $\omega\to 0$, i.e., at large distances. For a metal $|\epsilon(0)|\to\infty$ while for an insulator $\epsilon(0)$ is finite. The static value of the dielectric function of LiF, reached at frequencies $\omega<10^{-5}$ a.u., is $\epsilon(0)\sim$ 9.1 while the ''optical value'' ($\omega\sim 10^{-2}-10^{-1}$ a.u.) is $\epsilon(\infty)\sim 1.96$ [26]. In between these two limits, $\epsilon(\omega)$ varies strongly with ω. It should be noted that in the optical limit of the dielectric response, $\epsilon(\omega)=\epsilon(k\to 0,\omega)$, only delocalized and long-range polarization effects are included. Local perturbation of the surface due to the interaction with the HCI does not enter $\epsilon(\omega)$. It has earlier been argued that for relevant neutralization distances and times ($\simeq 10^{-14}$ s $\simeq 10^{-3}$ a.u.), the ω-dependent dielectric function $\epsilon(\omega)$, rather than the static limit $\epsilon(0)$, should be used when calculating the image potentials [27].

The experimental values of $\epsilon(\omega)$, as given by Palik and Hunter [26], are well represented by

$$\epsilon(\omega)=\epsilon(0)+\{\epsilon(\infty)-\epsilon(0)\}\frac{\omega^2}{\omega(\omega+i\gamma)-\omega_0^2}, \tag{13}$$

where $\epsilon(0)$ is the static value and $\epsilon(\infty)$ the optical value. The dielectric function (13) has a resonancelike behavior where the resonance is positioned at ω_0 and has a width γ. The real part and imaginary part of $\epsilon(\omega)$ are displayed in Figs. 2(a) and 2(b), respectively. The theoretical values are obtained from Eq. (13) using $\omega_0=1.39\times 10^{-3}$ a.u. and $\gamma=9.0\times 10^{-5}$ a.u.

We analyze the dependence of the image potentials on $\epsilon(\omega)$ for different interaction times and neutralization distances. To this end, we write the potential in the form

$$V_{pe}^I(z,R_z)\equiv V_{pe}^I(x=R_x,y=R_y,z,R_z) = \chi(z,R_z)\frac{Qq(z)}{|z+R_z|} \tag{14}$$

where the dielectric response function $\chi(z,R_z)$ represents a ''weighted'' value of the ratio $(\epsilon(\omega)-1)/(\epsilon(\omega)+1)$ in the integrand of Eq. (10) and has, for an insulator, at infinitely large distances the static limit

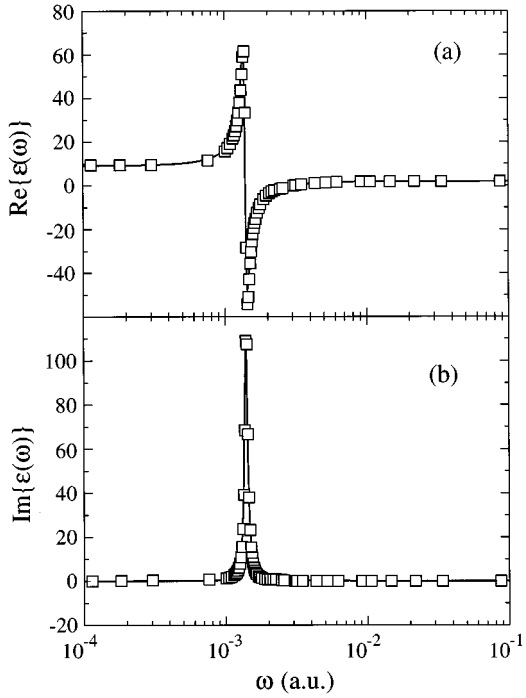

FIG. 2. Dielectric function $\epsilon(\omega)$ for LiF as a function of the frequency ω. The squares are experimental values from Palik and Hunter [26] and the solid line is obtained from Eq. (13) with $\omega_0=1.39\times10^{-3}$ a.u. and $\gamma=9.0\times10^{-5}$ a.u. (a) Real part of $\epsilon(\omega)$, (b) imaginary part of $\epsilon(\omega)$.

$$\chi(z,R_z)\xrightarrow[z,R_z\to+\infty]{}\frac{\epsilon(0)-1}{\epsilon(0)+1}. \tag{15}$$

We note that the limits of the response are given by $0\leqslant\chi\leqslant1$ where the upper limit $\chi=1$ is reached for a metal.

For finite z and R_z, χ is given by

$$\chi(z,R_z)=\frac{V^I_{pe}(z,R_z)|z+R_z|}{Qq(z)}. \tag{16}$$

In this work we treat two cases: grazing incidence (finite $\vec{v}_{||}$, $v_z\to0$) and normal incidence ($\vec{v}_{||}\to0$, finite v_z). In the former case Eq. (10) becomes [25]

$$V^I_{pe}(\vec{r},\vec{R})=\frac{Qq(z)}{2\pi}\int\frac{d\vec{K}}{K}e^{i\vec{K}\cdot(\vec{\rho}-\vec{v}_{||}t)}e^{-K(|z|+|R_z|)}\times\left\{\frac{\epsilon(\vec{K}\cdot\vec{v}_{||})-1}{\epsilon(\vec{K}\cdot\vec{v}_{||})+1}\right\}, \tag{17}$$

while in the latter case Eq. (10) becomes

$$V^I_{pe}(\vec{r},\vec{R})=Qq(z)\int_0^\infty dKJ_0(K\rho)e^{-K(|z|+|R_z|)}\times\left\{\frac{\epsilon(iK|v_z|)-1}{\epsilon(iK|v_z|)+1}\right\}. \tag{18}$$

The response function χ, governing the image potentials, behaves differently for the cases of normal incidence and grazing incidence. In Fig. 3 we display $\chi(z,R_z)$ as a function

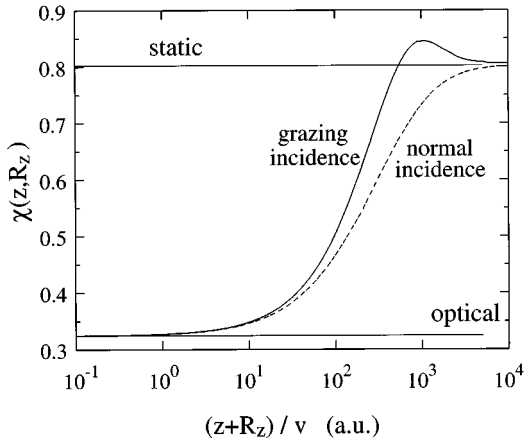

FIG. 3. Response function $\chi(z,R_z)$ as a function of $(z+R_z)/v$, where z is the distance between the electron and the surface while the projectile is at distance R_z and has a velocity v. The solid line is for grazing incidence ($v=|\vec{v}_{||}|$) and the dashed line is for normal incidence ($v=|v_z|$). The upper solid line is the static limit $\{\chi(z,R_z)=[\epsilon(0)-1]/[\epsilon(0)+1]\}$ and the lower solid line is the optical limit $\{\chi(z,R_z)=[\epsilon(\infty)-1]/[\epsilon(\infty)+1]\}$.

of the reduced variable $(z+R_z)/v$ for normal ($v=|v_z|$) as well as grazing ($v=|\vec{v}_{||}|$) incidence together with the optical and static limits of χ. We note that for the first capture $(z+R_z)$ is usually of the order of 10 a.u.. In grazing incidence measurements of the image energy gain the parallel velocity is typically in the 0.1 a.u. range which yields $(z+R_z)/v\sim10^2$. In normal incidence measurements typical perpendicular velocities are of the order of 0.01 a.u. and $(z+R_z)/v\sim10^3$. From Fig. 3 it is clear that in this region $[(z+R_z)/v\sim10^2-10^3]$ the fluctuations of $\epsilon(\omega)$ strongly affects the shape of $\chi(z,R_z)$ and neither the static nor the optical limit are good approximations.

The self-image potential for the electron, entering the electronic surface potential [Eq. (2)], is given in terms of χ by

$$V^{SI}_e(z)=\chi(z,R_z=z)\left(-\frac{q^2(z)}{4z}\right). \tag{19}$$

The localized positive charge in the surface, produced by the transfer of the electron to the HCI, is screened by the dynamic response. This contribution to the electronic surface potential in Eq. (2) is

$$V_{sc}(\vec{r})=\frac{1}{|\vec{r}|}a_M(z)\chi(z,0)q^2(z), \tag{20}$$

with the correct asymptotic behavior

$$\lim_{z\to\infty}[V_{sc}(x=0,y=0,z)]=\frac{\chi(z,0)}{z}. \tag{21}$$

The lattice and the surrounding electron cloud are polarized and this is accounted for by the screening potential $V_{sc}(\vec{r})$. Near the surface $V_{sc}(\vec{r})$ approximates the Mott-Littleton in-

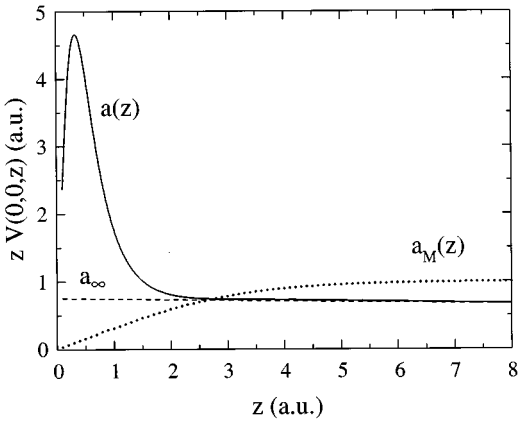

FIG. 4. Function $a(z)$ in Eq. (22) for LiF (solid line), the corresponding function $a_M(z)$ for the Madelung potential (dotted line), and the asymptotic form $a_\infty \simeq 1-\chi(z,0)+\chi(z,z)/4$ (dashed line) as a function of z, the distance between the electron and the surface.

teraction [28]. The inclusion of $a_M(z)$ in Eq. (20) does not only prevent $V_{sc}(0,0,z)$ from diverging close to the surface ($z\rightarrow 0$) but also ensures that for a metal ($\chi\rightarrow 1$) the contribution from the interaction with a crystal surface, V_M+V_{sc}, vanishes. We note that χ in Eq. (19) as well as Eq. (21) should be related to the time dependence of the charge transfer, as determined by the local velocity of the electron. Since this is presently not feasible, we choose the velocity of the projectile which provides an estimate for the relevant time scale.

The asymptotic behavior of $V_e(\vec{r})$ is of particular interest for analytic estimates of critical distances for charge transfer. To this end we define a function $a(z)$ such that

$$a(z)\equiv -zV_e(x=0,y=0,z). \tag{22}$$

The function $a(z)$ for a LiF crystal is displayed in Fig. 4 together with the corresponding function for the Madelung potential, $a_M(z)$ [Eq. (9)], and the asymptotic form $\lim_{z\rightarrow\infty}\{a(z)\}=a_\infty\simeq 1-\chi(z,R_z=0)+\chi(z,R_z=z)/4$. The χ-dependent behavior of the function $a(z)$ for insulators is quite different from the case of a metal for which $\chi\rightarrow 1$ and $a(z)\simeq 1/4$. For metals the long-range behavior is dominated by the electronic self-image while for an insulator the asymptotic interaction between the electron and the target can vary between Coulombic [small dielectric response, $a(z)\simeq 1$] and self-image-like [large dielectric response, $a(z)\simeq 1/4$].

Finally, in Eq. (1), the Coulomb interaction between the projectile and the electron is denoted by

$$V_{pe}(\vec{r},\vec{R})=\frac{-Qq(z)}{|\vec{r}-\vec{R}|}. \tag{23}$$

For sequential capture and distances comparable to the radius of the charge cloud of previously captured electrons, Slater screening should be taken into account [2,4,27]. Here, we focus our attention on the first stage of capture.

The six contributions to the total electronic surface potential $V(\vec{r},\vec{R})$ [Eqs. (1) and (2)] have now been explicitly described. The COB estimate for R_c for first capture will be made for the so-called ''top position,'' where the

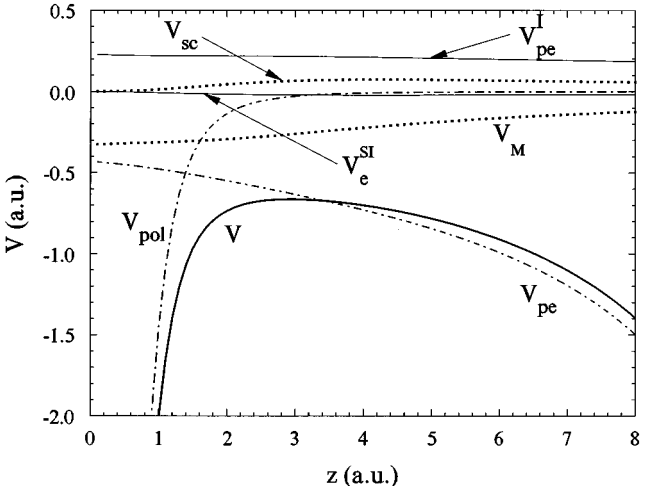

FIG. 5. Electronic potential $V(z,R_z)$ calculated from Eq. (24) for grazing incidence with velocity $|\vec{v}_{||}|=0.1$ a.u., charge $Q=6$, and position $R_z=12$ a.u. The total potential as well as its six contributions are shown.

projectile is located on top of the lattice site of the halide, i.e. along the z axis in our coordinate system. Along the line $\vec{r}=(0,0,z)$, with $\vec{R}=(0,0,R_z)$ the potential $V(\vec{r},\vec{R})$ can be simplified to

$$\begin{aligned} V(z,R_z)=&-\frac{\alpha_{pol}}{2(z^2+c^2)^2}-\frac{a_M(z)q^2(z)}{z}\{1-\chi(z,0)\}\\ &-\frac{1}{4z}\chi(z,z)q^2(z)+\chi(z,R_z)\frac{Qq(z)}{|R_z+z|}-\frac{Qq(z)}{|R_z-z|}\\ =&-\frac{a(z)}{z}+\chi(z,R_z)\frac{Qq(z)}{|R_z+z|}-\frac{Qq(z)}{|R_z-z|}. \end{aligned} \tag{24}$$

The potential in Eq. (24) is shown in Fig. 5 for grazing incidence with velocity $|\vec{v}_{||}|=0.1$ a.u. and charge $Q=6$ positioned at $R_z=12$ a.u. outside the surface. The breakdown of the potential into its six contributions is also displayed. It is clear from Fig. 5 that the shape of the total potential is dominated by the polarization potential $V_{pol}(\vec{r})$ close to the surface and by the Coulomb potential $V_{pe}(\vec{r},\vec{R})$ close to the projectile. The height of the potential at the saddle point is also affected by the Madelung potential $V_M(\vec{r})$ and the image potential $V^I_{pe}(\vec{r},\vec{R})$. The small dielectric response reduces the influence of all the image contributions as compared to a metal. In particular, the contributions $V_{sc}(\vec{r})$ and $V_e^{SI}(z)$ are small in magnitude. The exact forms of $V_{sc}(\vec{r})$ and $V_e^{SI}(z)$ close to the surface are not known but they must approach a finite value for $z\rightarrow 0$, which we incorporate through the exponential prefactor $f(z)$. This inclusion does not significantly affect the shape and the position of the saddle nor does it alter the long range behavior of the potentials.

The total potential $V(\vec{r},\vec{R})$ is displayed in Fig. 6 in planes parallel to the surface (z fixed) for a grazing incidence HCI at $\vec{R}=(0,0,12)$, with charge $Q=6$ and velocity $|\vec{v}_{||}|=0.1$ a.u. In Fig. 6(a) we show $V(\vec{r},\vec{R})$ for $z=1.0$ a.u., i.e., very close to the surface. The dominant contributions are $V_{pol}(\vec{r})$ and

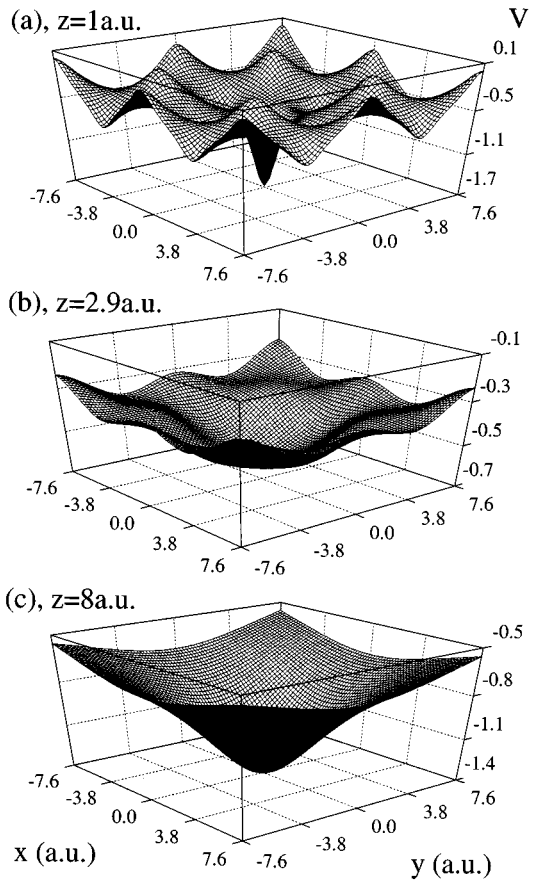

FIG. 6. Electronic potential $V(\vec{r},\vec{R})$, from Eq. (1), in planes parallel to the surface of the crystal. The projectile is at position $\vec{R}=(0,0,12)$ a.u., has charge $Q=6$, and is grazing incident with velocity $|\vec{v}_{||}|=0.1$ a.u. (a) Plane at $z=1.0$ a.u. (b) Plane at $z=2.9$ a.u. (c) Plane at $z=8.0$ a.u.

$V_M(\vec{r})$ and the effect of the ionic centers in the crystal is clearly visible. In Fig. 6(b) the plane is at $z=2.9$ a.u., which is the position of the top of the barrier (Fig. 5). The potential in Fig. 6(b) has a pronounced minimum at $(x=0, y=0)$ and the effect of the ionic centers is still visible. In Fig. 6(c) the potential is shown for $z=8.0$ a.u., i.e., close to the projectile, and, as expected, the shape of the potential is completely dominated by $V_{pe}(\vec{r},\vec{R})$.

III. CRITICAL DISTANCES AND QUANTUM NUMBERS

In the COB model, the neutralization sequence begins at a critical distance $R_z=R_c$ where the barrier between the ion and the surface falls below the highest-lying occupied target levels (Fermi edge) and the electron transfer becomes classically allowed. This model implicitly assumes that at $R_z=R_c$ the electronic states have become sufficiently polarized such that they explore the region of the saddle. In this section we present estimates for R_c and for quantum numbers n_c of the levels the electron will be captured into for insulators in the ''top geometry,'' which represents the most favorable configuration for charge transfer. Corrections due to the polarization of the $2p$ orbital of F^- and the dependence on the lateral position with respect to the HCI will be discussed in the next section.

At the distance of the first capture, the top of the barrier is equal to the shifted target levels,

$$V(z_s,R_c)=E_T=-W+\frac{Q}{R_c}[\chi(0,R_c)-1]q(0) \tag{25}$$

where W is the work function. The last term in Eq. (25), which is absent for a metal ($\chi\to 1$), describes the shift of the target levels in the field of the projectile. The position of the saddle (z_s) is obtained from

$$\left.\frac{\partial V(z,R_c)}{\partial z}\right|_{z=z_s}=\frac{a(z_s)}{z_s^2}-\frac{1}{z_s}\frac{\partial a(z_s)}{\partial z}+\frac{\partial \chi(z_s,R_c)}{\partial z}\frac{Qq(z_s)}{|R_c+z_s|}+\frac{Q\chi(z_s,R_c)}{|R_c+z_s|}\frac{\partial q(z_s)}{\partial z}-\frac{Qq(z_s)}{(R_c+z_s)^2}\chi(z_s,R_c)-\frac{Qq(z_s)}{(R_c-z_s)^2}-\frac{Q}{|R_c-z_s|}\frac{\partial q(z_s)}{\partial z}=0. \tag{26}$$

It is important to note that Eqs. (25) and (26) represent an implicit relation for R_c and z_s which must be solved by iteration. In order to compare the solutions with previous results for metals, it is useful to make an expansion of these expressions in powers of (z_s/R_c) (i.e., in the limit of large charges Q). To zeroth order in (z_s/R_c), Eq. (26) gives

$$z_s\simeq R_c\left[\frac{a(z_s)}{Qb(z_s,R_c,Q)}\right]^{1/2}, \tag{27}$$

where

$$b(z_s,R_c,Q)=q(z_s)\{1+\chi(z_s,R_c)\}+R_c\frac{\partial q(z_s)}{\partial z}\times\{1-\chi(z_s,R_c)\}-R_cq(z_s)\frac{\partial\chi(z_s,R_c)}{\partial z}+\frac{R_c^2}{Qz_s}\frac{\partial a(z_s)}{\partial z}. \tag{28}$$

Neglecting terms of order $(z_s/R_c)^2$ and higher, the critical distance for the onset of capture is given from Eq. (25) by

$$R_c\simeq\frac{1}{W}\left[Q\{q(z_s)\{1-\chi(z_s,R_c)\}+q(0)\{\chi(0,R_c)-1\}\}+\sqrt{Q}\sqrt{a(z_s)b(z_s,R_c,Q)}\left\{\frac{q(z_s)\{1+\chi(z_s,R_c)\}}{b(z_s,R_c,Q)}+1\right\}\right]. \tag{29}$$

It is important to note that only for a velocity independent response χ (such as the optical or static limit) and a z-independent charge q Eq. (29) gives an explicit expression for R_c. For a metal $\chi\to 1$, $a(z)\simeq 1/4$, $q(z)=1$, and hence $b(z_s,R_c,Q)=2$, which when used in Eq. (29) give the previously known critical distance for a metal [4]:

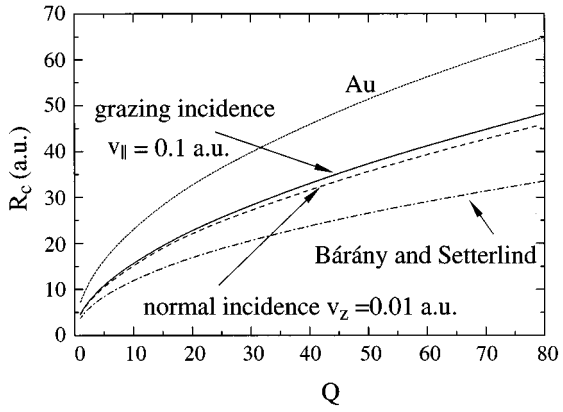

FIG. 7. Critical distance R_c for first capture as a function of the charge Q of the projectile. The solid line is for LiF ($W=12.3$ eV), calculated from Eq. (25), for a grazing incidence projectile with velocity $|\vec{v}_{||}|=0.1$ a.u. The dashed line is for normal incidence with $|v_z|=0.01$ a.u. The dash-dotted line is for LiF from Bárány and Setterlind [see Eq. (31)] while the dotted line is for gold ($W=5.3$ eV).

$$R_c \simeq \frac{\sqrt{2Q}}{W}. \tag{30}$$

In Fig. 7 we show the critical distance R_c for grazing incidence with $|\vec{v}_{||}|=0.1$ a.u. and for normal incidence with $|v_z|=0.01$ a.u. Also given is the critical distance from Bárány and Setterlind [29–31] as well as the critical distance of the COB model for gold [4]. Bárány and Setterlind [29–31] have derived a general formula for the critical distance for capture from metals, semiconductors, and insulators as [31]

$$R_c=\frac{[2Q\epsilon(8i+\epsilon-1)]^{1/2}}{(\epsilon+1)W}, \tag{31}$$

where ϵ is a constant dielectric function (static or optical limit) and i is the positive charge left behind on the surface. For our comparison we have chosen $i=1$ and $\epsilon=9.1$. The difference between the R_c's for LiF as seen in Fig. 7 can be explained by two effects. First, the velocity dependent response function χ is in this velocity regime ($|\vec{v}_{||}|=0.1$ or $|v_z|=0.01$) far from any of the limits (static or optical) as discussed earlier. Second, the interaction with the ionic crystal is here treated through a position dependent potential $-a_M(z)/z$ while Bárány and Setterlind use a pure Coulomb interaction $-1/z$. The fact that our calculations for normal incidence with $v_z=0.01$ a.u. yield almost identical results to those for grazing incidence with $v_{||}=0.1$ a.u. is a coincidence. It is clear from Fig. 7 that the onset of capture occurs at considerably smaller distances from an insulator like LiF than from a metal like Au. The effect of the much larger work function of LiF dominates over the effect of a smaller response function χ.

As the first electron is transferred from the target to the projectile, it ends up in a level with a critical quantum number n_c. Since the effect of a fractional ionicity in the crystal is negligible far from the surface [$q(R_c)\simeq 1$], the energy shift of projectile levels can be expressed as

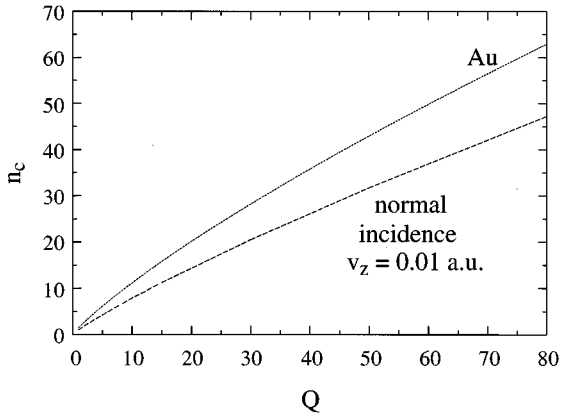

FIG. 8. Critical quantum number n_c for first capture as a function of the charge Q of the projectile. The dashed line is for normal incidence with $|v_z|=0.01$ a.u. The dotted line is the quantum number n_c for gold.

$$E_n(R_z)=-\frac{Q^2}{2n^2}+\frac{(Q-1/2)}{2R_z}\chi(R_z,R_z)+V_{pol}(R_z) - \frac{a_M(R_z)}{R_z}\{1-\chi_{stat}\}, \tag{32}$$

where the last term, absent for a metal, describes the shift of the projectile levels in the crystal field. The expression for the energy shift due to the crystal field is valid in the case of normal incidence while for grazing incidence the lateral displacement of the positive charge must be taken into account. The dielectric screening of the hole is given by the static limit χ_{stat} of the surface response function.

From the condition that E_n equals the energy of the target levels E_T [Eq. (25)] at the point of first capture, the critical quantum number follows as

$$n_c(R_c)=Q\left[2\left(W+\frac{Q[1-\chi(0,R_c)]q(0)}{R_c} +\frac{(Q-1/2)\chi(R_c,R_c)}{2R_c}+V_{pol}(R_c) -\frac{a_M(R_c)}{R_c}\{1-\chi_{stat}\}\right)\right]^{-1/2}. \tag{33}$$

We note that with a large dielectric response ($\chi\rightarrow 1$) the correct expressions for a metal [4] can be obtained as special cases of Eqs. (32) and (33).

In Fig. 8 the critical quantum number n_c from Eq. (33) is given for LiF and normal incidence with $|v_z|=0.01$ a.u. together with the corresponding values for Au. Clearly, the first electron captured from LiF ends up in a lower level than the first one captured from Au. Once again the effect of the larger work function dominates. For grazing incidence at $v_{||}=0.1$ a.u. assuming no lateral displacement, we find that the resulting n_c levels into which the electron is captured are almost identical to the ones in Fig. 8 for normal incidence. It should be noted that the extension of Eqs. (29) and (33) to multielectron capture is not straightforward: with each additional electron transfer, the corresponding Madelung contri-

bution changes and depends on the history of previous capture events, i.e., on the location of lattice sites from which capture occurred.

IV. CTMC SIMULATIONS

Unlike metals described by a jellium, the potential surface in front of a LiF surface (Fig. 6) does not possess rotational symmetry about the surface normal passing through the projectile position. The lack of symmetry is particularly obvious when the ion does not approach the surface in a ''top'' configuration relative to a halide discussed above or when electrons from neighboring sites have already been captured resulting in an anisotropic charge distribution in the surface. Under these conditions, the normal as well as lateral position of the saddle point becomes a complicated function of the ionic position and the ''reaction coordinate'' for the overbarrier transition is no longer a straight line. It is therefore convenient to perform classical-trajectory Monte Carlo (CTMC) simulations [16,17] for the overbarrier transition. These permit the determination of effective critical distances R_c (which may turn out to be somewhat different from the estimates given above) and projectile binding energies (i.e., n_c). Moreover, they yield capture and loss rates which enter the rate equations for the populations of different n shells in COB simulations [4]. We have therefore performed an electron trajectory simulation of capture from a LiF surface to a slow approaching HCI. Somewhat similar simulations have previously been undertaken for metals by Bardsley and Penetrante [32]. They calculated, using field-emission theory, the current of electrons produced by the electric field that the HCI creates at the surface of the metal. To our knowledge, the present simulations are the first treating the time evolution of valence electrons, initially localized around ionic centers, in the presence of an approaching slow HCI.

Our calculation is based on a CTMC method in which a restricted microcanonical ensemble of initial conditions representing the $2p$ electrons of F ions is generated. The electrons are in the potential V_e with binding energy $W=12.3$ eV and with a classical atomic angular momentum L restricted to $[l,l+1]$ with quantum number $l=1$. In agreement with the concept of fractional ionicity, the electronic trajectories are not completely localized around the F ions but undertake excursions to the neighboring Li ions.

In the simulation presented here, we consider normal incidence with a constant $v_z=0.004$ a.u. This velocity corresponds to a typical lower limit set by the image charge acceleration. We choose the initial position R_z of the projectile such that $R_z \gg R_c$, i.e., the polarization of the target electron by the incident ion is taken into account. The lateral position of the ion is randomized over the crystal and all neighboring F^- ions from which capture is possible are included. As the ion approaches the surface, the position of the electron is monitored. When the electron crosses the top-geometry saddle ($z>z_s$) (''first passage'') and thereafter reaches the ion ($z>R_z$), it is counted as captured. At a given value of R_z, the number of captured electrons $N_c(R_z)$ is calculated as the ratio of the number of trajectories for which the electron is captured at some point during the simulation (before the R_z) to the total number of trajectories.

The results for $N_c(R_z)$ for $Q=6$ and $Q=15$ are shown as solid lines in Figs. 9(a) and 9(b), respectively. Note, that at small distances N_c becomes greater than unity due to capture of electrons from different F^- sites. In fact, by the time $N_c \sim 1$, electrons from sites corresponding to a surface section with a diameter of about $6d-8d$ contribute to electron capture. We also record the total number of electrons which is in the vicinity of the projectile, $N_{tot}(R_z)$ at a given distance. The latter number takes into account the competition between capture and loss. It accounts for the fact that electrons may pass over the saddle back to the surface, if no restrictions on energy matching or blocking of occupied sites in the insulator surface are imposed. The latter provides, therefore, an estimate for maximum loss effects. Results for $N_{tot}(R_z)$ are also shown in Figs. 9(a) and 9(b), which are considerably smaller than $N_c(R_z)$, indicating that a significant fraction of electrons is lost. Capture and loss rates can be obtained from the slopes of these curves.

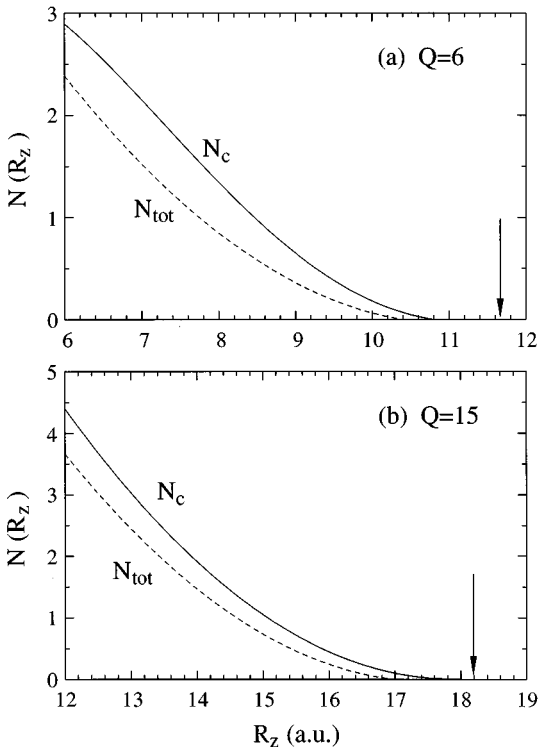

FIG. 9. Number of captured electrons $N_c(R_z)$ for (a) $Q=6$ and (b) $Q=15$ is displayed as solid lines. The number of electrons after accounting also for loss (see text), $N_{tot}(R_z)$, is shown as dashed lines. The critical distances given by Eq. (25) using $W=12.3$ eV are indicated by arrows.

An important observation refers to the comparison to the estimate of R_c within the COB model for insulators [Eq. (29)], indicated by arrows in Fig. 9. While capture is energetically permitted at the critical distance R_c, significant capture does not set in until the ion has moved closer to the surface. In particular, we find that the total number of captured electrons reaches 1 when the ion is about 3 a.u. closer to the surface than what the COB estimate predicts. This correction can be related to two effects: the statistically significant contributions from projectile positions different from the top position and the finite response time for the polarization of the $2p$ orbital. The latter can be easily interpreted in terms of classical trajectories (Fig. 10): the initial $2p$ elec-

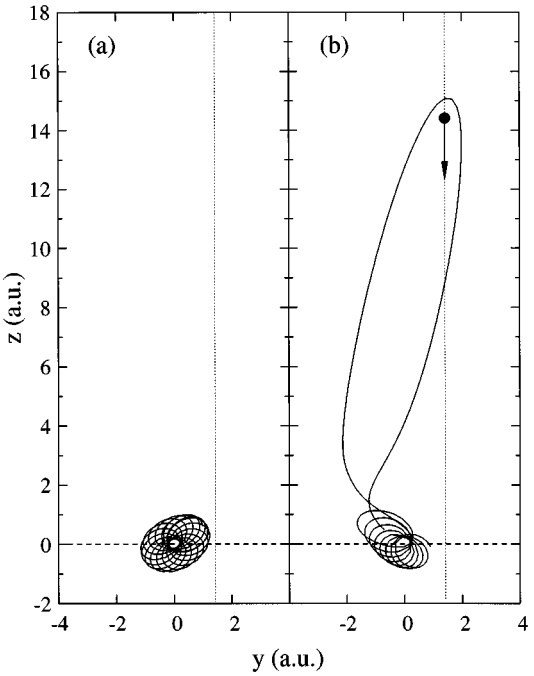

FIG. 10. Example of a classical trajectory of an electron as an HCI with $Q=15$, $v_z=0.004$ a.u., $R_x=0.11$ a.u., and $R_y=1.41$ a.u. approaches the surface. (a) The initial polarization of the classical ''$2p$'' orbit at a distance $R_z\sim 27$ a.u. from the surface, and (b) the more pronounced polarization followed by the passage over the saddle into the projectile at $R_z\sim 14.5$ a.u. The dashed line shows the position of the surface, the dotted line the R_y coordinate of the ion, and the filled circle in (b) indicates the position of the ion.

tron is in a low-eccentricity orbit [Fig. 10(a)]. In order to explore the saddle region, the orbit must be significantly polarized. Although transfer is energetically allowed, the electron needs, in addition, enough momentum along the ''reaction'' coordinate for barrier crossing. As the strength of the perturbation increases, the orbit of the electron is eventually sufficiently polarized to have enough linear momentum in the required direction to escape along the saddle [Fig. 10(b)]. As discussed below, this correction to the critical distance for insulators can be easily incorporated in applications of the COB model to the energy gain, to which we will refer to as the modified COB model. These corrections will also affect conclusions regarding the efficiency of hollow-atom formation. It should be noted that this correction is specific to localized target electrons and does not apply to metals.

V. ENERGY GAIN

As the HCI approaches the surface it experiences image acceleration due to the polarization of the surface. The resulting energy gain, which for HCIs with low velocities is considerable, has been measured for insulators as well as metals [5,6,33,34]. This experimental image energy gain gives information on the distances at which the neutralization process of the HCI sets in. The projectile image potential is

$$V_p^{SI}(R_z)=\chi(z=R_z,R_z)\left(-\frac{Q^2}{4R_z}\right), \tag{34}$$

where χ is the dielectric response function. The image energy gain at the point of first capture is given in terms of the ionic potential by

$$\Delta E_1^I=V_p^{SI}(\infty)-V_p^{SI}(R_c)=\frac{Q^2}{4R_c}\chi(R_c,R_c). \tag{35}$$

For metals ΔE_1^I was shown to be the dominant contribution to the total energy gain ΔE, which was calculated in a full COB simulation as well as from the so called staircase model [3,4]. Within the staircase model, the charge is assumed to change instantaneously from Q to $Q-1$ at $R_c(Q)$, from $Q-1$ to $Q-2$ at $R_c(Q-1)$, etc. until complete neutralization is reached. An implicit assumption of the staircase model is that electron capture proceeds sequentially, i.e., simultaneous multiple capture plays only a minor role. Accordingly, within the staircase model the total energy gain for a metal is related to the gain at the point of first capture by

$$\Delta E\simeq 4\Delta E_1^I/3, \tag{36}$$

which was shown to be a reasonable approximation to the result of a full simulation, somewhat underestimating ΔE for $Q\lesssim 10$ and somewhat overestimating ΔE for very large charge states $Q\gtrsim 20$ [35].

For an insulator surface we have a different scenario due to the more localized character of the electrons initially bound to the crystal. The charge transfer from the crystal to the projectile causes a local charge-up of the surface. The presence of these positive charges decelerates the HCI which, to some extent, counteracts the effect of the subsequent image acceleration. During the interaction time of one HCI with the surface the positive charges do not migrate in the crystal.

The total energy change of the HCI approaching the insulator surface is hence

$$\Delta E=\Delta E^I+\Delta E^D, \tag{37}$$

where ΔE^D is the energy loss of the ion caused by the local charge-up.

Under the assumption that the staircase model is valid we have, for an insulator, a total image energy gain of

$$\Delta E^I=\Delta E_1^I+\sum_{i=1}^{Q-1}\frac{(Q-i)^2}{4}\left[\frac{\chi(R_c(Q-i),R_c(Q-i))}{R_c(Q-i)}-\frac{\chi(R_c(Q-[i+1]),R_c(Q-[i+1]))}{R_c(Q-(i+1))}\right]. \tag{38}$$

The major contribution to the image energy gain is from the trajectory up to the first capture, ΔE_1^I. The energy loss ΔE^D is obtained by a similar staircase approximation where we calculate the sequence of momentum transfers due to the repulsive force between the instantaneous ionic charge $Q-i$ and the charged-up surface with charge i. Consequently, the energy loss due to deceleration is, within the staircase model,

$$\Delta E^D = \sum_{i=1}^{Q-1} \left[-\left(\frac{v_z(i)}{|\vec{v}_{||}|} \right) T(i) + \left(\frac{1}{2M|\vec{v}_{||}|^2} \right) T^2(i) \right], \tag{39}$$

where M is the mass of the ion, $v_z(i)$ is the perpendicular velocity which changes with each capture, and

$$T(i) = \frac{(Q-i)\{1-\chi(R_c(Q-i),0)\}S(i)}{R_c(Q-i)}. \tag{40}$$

In Eq. (40) the factors $S(i)$ are given by

$$S(i) = \sum_{j=1}^{i} \frac{D(j,i)}{[R_c^2(Q-i)+D^2(j,i)]^{1/2}} - \sum_{j=1}^{i-1} \frac{D(j,i-1)}{[R_c^2(Q-i)+D^2(j,i-1)]^{1/2}} \tag{41}$$

with

$$D(j,i) = \sum_{k=j}^{i} \Delta R_{||}(Q-k). \tag{42}$$

To find the distances $\Delta R_{||}(Q-k)$ the ion travels along the surface between two consecutive capture events, i.e., the two steps of the staircase, k and $k+1$, we assume a grazing trajectory. As the ion travels the distance $\Delta R_{||}(Q-k) = R_{||}(Q-k) - R_{||}(Q-(k+1))$ along the surface, the distance to the surface is reduced by $\Delta R_c(Q-k) = R_c(Q-k) - R_c(Q-(k+1))$, i.e., the difference between the critical distances of two adjacent charge states. Accordingly, $\Delta R_{||}(Q-k) = \Delta R_c(Q-k)|\vec{v}_{||}|/v_z(k)$, where the initial ratio $v_z(0)/|\vec{v}_{||}|$ is typically of the order 2×10^{-2} a.u. in grazing incidence collisions. Because of the large mass of the ion ($M \sim 10^4$ a.u.) the first term in the sum in Eq. (39) will dominate the deceleration.

In order to evaluate Eq. (37), we use the R_c values from Eq. (32), corrected for the shift by 3 a.u. as obtained from the CTMC simulations. In other words, we account for a delayed formation of hollow atoms. These corrected values enter also the evaluation of χ. Since both χ and R_c are smaller than for metals at a given charge state Q, the effect of the much larger work function of LiF is partially compensated. In fact, for grazing incidence with $|\vec{v}_{||}|$ of about 0.1 a.u., the two counteracting effects of acceleration and deceleration largely cancel out and the total energy change ΔE is close to ΔE_1^I. We note that the similarities between an insulator and a metal at this velocity, as discussed in Ref. [5] are, to some extent, fortuitous. At higher velocities and high charges Q, more pronounced differences develop: In Fig. 11 the image energy gain for first capture, ΔE_1^I from Eq. (35), and the staircase sequence including deceleration, ΔE from Eq. (37), are shown as functions of Q for $|\vec{v}_{||}| = 0.45$ a.u. for LiF, together with the corresponding values for Au. The major difference comes from the difference in work functions (for LiF $W = 12.3$ eV; for Au $W = 5.3$ eV), which is not compensated for to the same extent for higher velocities.

Our calculations suggest that the study of the velocity dependence of the energy gain for a fixed charge state might provide a measure for the differences in the neutralization dynamics of metals and insulators. Figure 12 illustrates the $|\vec{v}_{||}|$ dependence for a grazing incidence interaction of a $Q=6$ ion at LiF and gold surfaces. Results for both ΔE_1^I and ΔE are shown together with experimental data. While for a metal the energy gain is expected to be energy independent (as long as $v_{||} \ll v_F$), the energy gain is reduced for LiF with increasing velocity because of the varying ionic polarizability of the LiF surface. The deceleration to some extent weakens the dependence. A more detailed comparison with the data of Auth *et al.* [5] and Yan and Meyer [6] is shown in Fig. 13. We also show results for which the correction due to delayed onset of capture (see Sec. IV) is omitted. We find very good agreement with the data of Ref. [6] within the experimental uncertainty when the delay is taken into account, while the energy gain is lower when this correction is not included, in better agreement with the data of Ref. [5]. However, the significance of this agreement should be viewed with caution at present. For example, a small uncertainty in our calculations arises from the fact that the image plane has been assumed to be at the topmost layer. Furthermore, recent experimental data for the velocity dependence of the exit charge state of several neutral atoms and negative

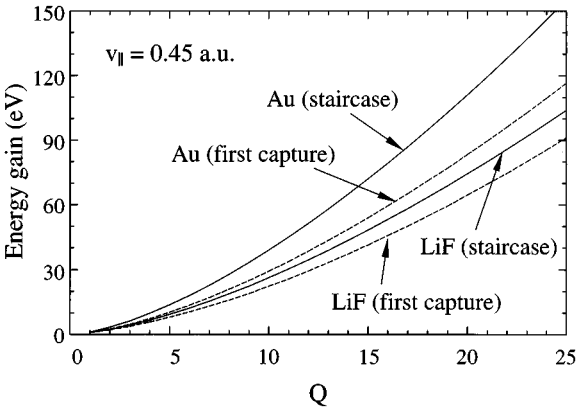

FIG. 11. Image energy gain at the point of first capture ΔE_1^I and total gain ΔE (staircase model) as a function of charge Q for gold and LiF. We assume grazing incidence with a parallel velocity of $|\vec{v}_{||}| = 0.45$ a.u. ΔE_1^I, dashed lines; ΔE, solid lines.

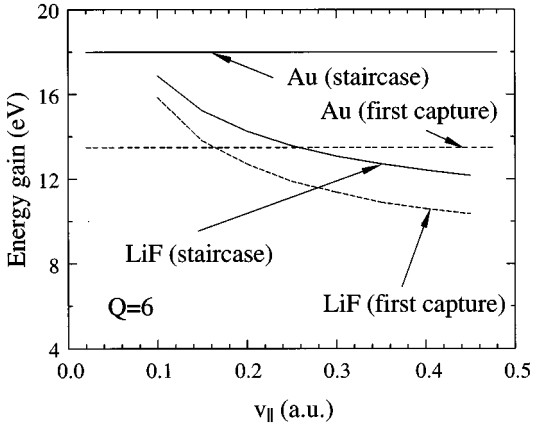

FIG. 12. Image energy gain at the point of first capture ΔE_1^I, and total gain ΔE (staircase model) for grazing incidence as a function of the parallel velocity $v_{||}$ for initial charge $Q=6$. The dashed lines are ΔE_1^I and the solid lines are ΔE.

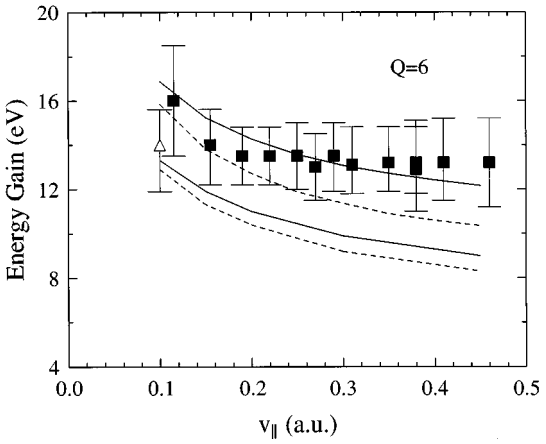

FIG. 13. Energy gain for LiF as a function of the velocity $v_{||}=|\vec{v}_{||}|$ for a grazing incidence HCI with initial charge $Q=6$. The dashed line is the image energy gain at the point of first capture, ΔE_1^I, and the solid line the total gain ΔE (staircase model). Experimental values from Yan and Meyer [6] are displayed as solid squares and the value from Auth *et al.*. [5] as an open triangle. The correction due to the delayed capture onset is included (excluded) in the upper (lower) curves.

ions [6] have not yet been satisfactorily explained. Further experimental and theoretical studies are therefore necessary to disentangle these different charge-transfer mechanisms.

VI. SUMMARY

We have formulated a classical overbarrier model for neutralization of highly charged ions near surfaces of insulators. We include the Madelung and polarization potentials in the description of the electronic potential of the target surface. Furthermore, the pronounced frequency-dependent $\epsilon(\omega)$ is included in the calculation of the image potentials.

For the neutralization process of the HCI in front of an ionic crystal, expressions for critical distances and quantum numbers for the first capture have been derived. In addition, electron-trajectory simulations have been performed for an insulator surface showing that the electron transfer is delayed, leading to corrections to the formula for critical distances for the onset of neutralization.

For grazing incidence we have calculated the image energy gain using a modified staircase model demonstrating the existence of a weak velocity dependence for LiF, due to the frequency-dependent polarizability of the surface, which is absent for a metal. The local charge-up of the insulator surface is taken into account as a deceleration of the HCI, which to some extent weakens the velocity dependence. Under the assumption that the staircase model is valid we obtain estimates of the total energy gain displaying a velocity dependence. Our calculated values are close to the experimental results for LiF.

In order to estimate the efficiency of the formation of hollow atoms for HCIs impinging on LiF and draw conclusions about KLL Auger transitions the complete capture sequence needs to be studied in more detail. A major difficulty is the complicated dependence of the potential on the history of the neutralization sequence, i.e., from which sites previous capture events have taken place. The local distribution of the microscopic charge-up may be crucial in determining the efficiency of hollow-atom formation.

ACKNOWLEDGMENTS

We are grateful to Q. Yan and F. Meyer for fruitful discussions and for providing us with their data prior to publication. L.H. would also like to thank A. Bárány for many helpful discussions. This work has been supported in part by the National Science Foundation and by the U.S. Department of Energy, Office of Basic Energy Sciences, Division of Chemical Sciences, under Contract No. DE-AC05-96OR22464 with Lockheed Martin Energy Research Corp. One of us (L.H.) would also like to acknowledge support from the Sweden-America Foundation, the Foundation Blanceflor Boncompagni-Ludovisi, née Bildt, and the Swedish Foundation for International Cooperation in Research and Higher Education.

[1] See, e.g., *The Physics of Electronic and Atomic Collisions, XVIII International Conference*, edited by T. Andersen, B. Fastrup, F. Folkmann, H. Knudsen, and N. Andersen (American Institute of Physics, New York, 1993).
[2] J. Burgdörfer, P. Lerner, and F. W. Meyer, Phys. Rev. A **44**, 5674 (1991).
[3] J. Burgdörfer and F. Meyer, Phys. Rev. A **47**, R20 (1993).
[4] J. Burgdörfer, in *Review of Fundamental Processes and Applications of Atoms and Ions*, edited by C. Lin (World Scientific, Singapore, 1993).
[5] C. Auth, T. Hecht, T. Igel, and H. Winter, Phys. Rev. Lett. **74**, 5244 (1995); C. Auth and H. Winter, Phys. Lett. A **217**, 119 (1996).
[6] Q. Yan and F. W. Meyer, Trans. Tech. Publ. Ltd. (Switzerland) (to be published).
[7] J. Limburg, S. Schippers, R. Hoekstra, R. Morgenstern, H. Kurz, F. Aumayr, and H. P. Winter, Phys. Rev. Lett. **75**, 217 (1995).
[8] T. Neidhart, F. Pichler, F. Aumayr, H. P. Winter, M. Schmid, and P. Varga, Phys. Rev. Lett. **74**, 5280 (1995).
[9] T. Neidhart, M. Sporn, M. Schmid, and P. Varga, Nucl. Instrum. Methods B **101**, 127 (1995).
[10] M. Vana, F. Aumayr, P. Varga, and H. P. Winter, Nucl. Instrum. Methods B **100**, 284 (1995).
[11] J-P. Briand, S. Thuriez, G. Giardino, G. Borsoni, M. Froment, M. Eddrief, and C. Sébenne, Phys. Rev. Lett. **77**, 1452 (1996).
[12] H. Ryufuku, K. Sasaki, and T. Watanabe, Phys. Rev. A **21**, 745 (1980).
[13] A. Bárány, G. Astner, H. Cederquist, H. Danared, S. Huldt, P. Hvelplund, A. Johnson, H. Knudsen, L. Liljeby, and K-G. Rensfelt, Nucl. Instrum. Methods B **9**, 397 (1985).
[14] A. Niehaus, J. Phys. B **19**, 2925 (1986).
[15] F. W. Meyer, S. H. Overbury, C. C. Havener, P. A. Zeijlmanns van Emmichoven, and D. M. Zehner, Phys. Rev. Lett. **67**, 723 (1991).
[16] R. Abrines and I. C. Percival, Proc. Phys. Soc. **88**, 861 (1966).

[17] R. E. Olson, in *Physics of Electronic and Atomic Collisions*, edited by H. B. Gilbody *et al.* (North-Holland, Amsterdam, 1987), p. 271.
[18] M. Karplus and R. N. Porter, *Atoms and Molecules. An Introduction for Students of Physical Chemistry* (W. A. Benjamin, Inc., New York, 1970).
[19] H. M. Evjen, Phys. Rev. **39**, 675 (1932).
[20] J. D. Levine and P. Mark, Phys. Rev. **144**, 751 (1966).
[21] C. Kittel, *Introduction to Solid State Physics* (Wiley, New York, 1971).
[22] Y. Wang, P. Nordlander, and N. H. Tolk, J. Chem. Phys. **89**, 4163 (1988).
[23] M. Piacentini and J. Anderegg, Solid State Commun. **38**, 191 (1981).
[24] W. Pong and C. S. Inouye, J. Electron Spectrosc. Relat. Phenom. **11**, 165 (1977).
[25] F. J. Garcia de Abajo and P. M. Echenique, Phys. Rev. B **46**, 2663 (1992).
[26] E. D. Palik and W. R. Hunter, in *Handbook of Optical Constants*, edited by E. D. Palik (Academic Press, New York, 1985), p. 675.
[27] J. Burgdörfer, C. Reinhold, L. Hägg, and F. Meyer, Aust. J. Phys. **49**, 527 (1996).
[28] N. Mott and M. Littleton, Trans. Faraday Soc. **34**, 485 (1938).
[29] A. Bárány (unpublished).
[30] A. Bárány and C. J. Setterlind, Nucl. Instrum. Methods B **98**, 184 (1995).
[31] A. Bárány and C. J. Setterlind, Heavy Ion Phys. **1**, 115 (1995).
[32] J. N. Bardsley and B. M. Penetrante, Comments At. Mol. Phys. **27**, 43 (1991).
[33] F. Aumayr, H. Kurz, D. Schneider, M. A. Briere, J. W. McDonald, C. E. Cunningham, and H. P. Winter, Phys. Rev. Lett. **71**, 1943 (1993).
[34] F. Meyer, L. Folkerts, H. O. Folkerts, and S. Schippers, Nucl. Instrum. Methods B **98** 441 (1995).
[35] C. Lemell, H. P. Winter, F. Aumayr, J. Burgdörfer, and F. Meyer, Phys. Rev. A **53**, 880 (1996).